Phys Chem Minerals (2007) 34:85–93
DOI 10.1007/s00269-006-0130-x

ORIGINAL PAPER

In search of the mixed derivative $\partial^2 M/\partial P\partial T$ ($M = G, K$): joint analysis of ultrasonic data for polycrystalline pyrope from gas- and solid-medium apparatus

G. D. Gwanmesia · I. Jackson · R. C. Liebermann

Received: 18 April 2006 / Accepted: 7 November 2006 / Published online: 12 December 2006

Abstract Elastic wave velocities for dense (99.8% of theoretical density) isotropic polycrystalline specimens of synthetic pyrope ($Mg_3Al_2Si_3O_{12}$) were measured to 1,000 K at 300 MPa by the phase comparison method of ultrasonic interferometry in an internally heated gas-medium apparatus. The temperature derivatives of the elastic moduli [$(\partial Ks/\partial T)_P = -19.3(4)$; $(\partial G/\partial T)_P = -10.4(2)$ MPa K^{-1}] measured in this study are consistent with previous acoustic measurements on both synthetic polycrystalline pyrope in a DIA-type cubic anvil apparatus (Gwanmesia et al. in Phys Earth Planet Inter 155:179–190, 2006) and on a natural single crystal by the rectangular parallelepiped resonance (RPR; Suzuki and Anderson in J Phys Earth 31:125–138, 1983) method but $|(\partial Ks/\partial T)_P|$ is significantly larger than from a Brillouin spectroscopy study of single-crystal pyrope (Sinogeikin and Bass in Phys Earth Planet Inter 203:549–555, 2002). Alternative approaches to the retrieval of mixed derivatives of the elastic moduli from joint analysis of data from this study and from the solid-medium data of Gwanmesia et al. in Phys Earth Planet Inter 155:179–190 (2006) yield $\partial^2 G/\partial P\partial T = [0.07(12),\ 0.20(14)] \times 10^{-3}$ K^{-1} and $\partial^2 K_S/\partial P\partial T = [-0.20(24),\ 0.22(26)] \times 10^{-3}$ K^{-1}, both of order 10^{-4} K^{-1} and not significantly different from zero. More robust inference of the mixed derivatives will require solid-medium acoustic measurements of precision significantly better than 1%.

Keywords Pyrope · Polycrystalline · Elasticity · Mixed derivative · Gas-medium apparatus

G. D. Gwanmesia (✉)
Department of Physics and Pre-Engineering,
Delaware State University,
Dover, DE 19901, USA
e-mail: ggwanmes@desu.edu

I. Jackson
Research School of Earth Sciences,
Australian National University,
Canberra ACT 0200, Australia

R. C. Liebermann
Department of Geosciences, Stony Brook University,
Stony Brook, NY 11794, USA

Introduction

Pyrope-rich garnet is a major component of crustal and upper mantle rocks such as peridotites and eclogites, and it constitutes about 15% by volume in garnet lherzolite models of the upper mantle. Experimental studies (e.g., Gasparik 1990, 1992) also show that pyrope ($Mg_3Al_2Si_3O_{12}$) forms complete solid solution with $Mg_4Si_4O_{12}$-majorite under the conditions of the transition zone of the Earth's mantle. Elastic moduli of garnets are relatively insensitive to composition and temperature compared to most other mantle phases (e.g., Stixrude and Lithgow-Bertelloni 2005). Accurate laboratory data on the elastic wave velocities of aluminous garnets and their pressure and temperature dependence are critical for evaluating different mineralogical and chemical models proposed for the Earth's interior by interpreting velocity and density models derived from seismic data. The mixed derivatives of the elastic moduli ($\partial^2 M/\partial P\partial T$: $M = K$ or G), are needed for robust extrapolation of laboratory-derived elasticity data to the conditions of the deep mantle. For example, the value of $K_0' = (\partial K/\partial P)_{P=0}$ to be used in a "hot" finite-strain equation of state, should be adjusted for the

high temperature T_0 at the foot of the mantle adiabat. For T_0 = 1,600 K, and a not unreasonable average value of 0.2×10^{-3} K^{-1} for $\partial^2 K/\partial P \partial T$, the required correction to K_0' would be +0.32, resulting in substantially higher calculated bulk sound speed and lower density at high pressure. However, such corrections are normally neglected because the only constraints come from scarce and sometimes contradictory experimental data (Spetzler 1970; Chen et al. 1998) and indirect inferences based on thermodynamic or lattice dynamical models (Isaak 1993; Jackson and Rigden 1996).

There is paucity of data on the high temperature elastic properties of pyrope–majorite garnets. Wang et al. (1998) obtained static P–V–T data for two synthetic polycrystalline specimens (Py_{100}, $Py_{62}Mj_{38}$) to 11 GPa and 1,163 K that yielded $(\partial K_T/\partial T)_P$ values for the two compositions. Suzuki and Anderson (1983) investigated the elasticity of natural pyrope single crystal by rectangular parallelepiped resonance (RPR) method to 1,000 K, at room pressure. Acoustic wave velocities of synthetic polycrystalline pyrope–majorite garnets ($Py_{50}Mj_{50}$; $Py_{20}Mj_{80}$) and of single crystal pyrope have been measured to ~1,100 K at room pressure by Brillouin spectroscopy (Sinogeikin and Bass 2002). Recently, Gwanmesia et al. (2006) have measured the elasticity of synthetic polycrystalline pyrope (Py_{100}) in a DIA-type cubic anvil apparatus to 10 GPa and temperatures of up to 1,273 K. However, there have been no studies of the mixed derivatives ($\partial^2 M/\partial P \partial T$: $M = K$ or G) of the elasticity of these mantle phases, because of difficulties associated with high-temperature pressure scales.

In this study, we present new data on the temperature dependence of elasticity of two synthetic polycrystalline specimens of pyrope ($Mg_3Al_2Si_3O_{12}$) to 1,000 K at 300 MPa. We compare our new elasticity data from the gas-medium apparatus with ultrasonic results presented by Gwanmesia et al. (2006) from the DIA-type cubic anvil apparatus, and also with data of Sinogeikin and Bass (2000) using Brillouin spectroscopy. We also discuss our efforts to constrain the mixed derivatives ($\partial^2 M/\partial P \partial T$) of the elastic moduli for pyrope by combining the ultrasonic data from two P–T ranges (Fig. 1)—the gas-medium apparatus (P = 300 MPa, T = 1,000 K) and the cubic anvil multi-anvil high pressure apparatus (P = 10 GPa, T = 1,273 K; Gwanmesia et al. 2006).

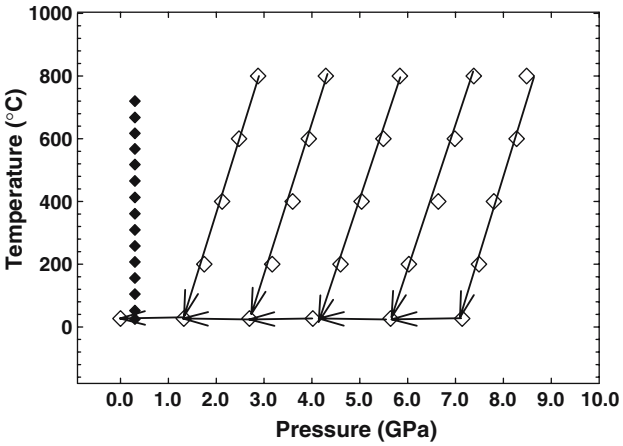

Fig. 1 Experimental P and T paths of unloading and cooling cycles in the S-wave and P-wave experiments: experiments conducted in the DIA-type cubic-anvil apparatus (SAM-85), in conjunction with Synchrotron X-radiation (*open diamond*). *Filled diamonds* represent data in the internally heated gas-medium apparatus

Experimental method

Sample preparation and characterization

The polycrystalline specimens of pyrope (Py_{100}) used in this study were hot-pressed in the 2,000 ton uniaxial split-sphere apparatus (USSA-2000) of the Kawai-type (Kawai and Endo 1970; Kawai et al. 1973; Yagi 2001) located in the High Pressure laboratory at Stony Brook at 9 GPa and 1,000°C for 1.5 h. The procedure for hot-pressing Py_{100} was identical to that used by Gwanmesia et al. (2006) and is described elsewhere in detail (Gwanmesia et al. 1990; Gwanmesia et al. 1993; Gwanmesia and Liebermann 1992). Briefly, fine powdered glass starting material is loaded into a Pt capsule, and then the capsule is sealed and surrounded by cold-pressed NaCl inside a graphite resistance furnace within the high-pressure cell assembly. Gwanmesia et al. (1992) showed that NaCl minimizes non-hydrostatic stress on samples during hot-pressing, yielding specimens that are generally cylindrical in shape. The pyrope polycrystalline specimens that were hot-pressed for this study were of about 3 mm in diameter and 2–3 mm long (Table 1). The samples were substantially larger than those used in the Gwanmesia et al. (2006) which were about 2 mm in diameter and 1 mm in length. The recovered specimens were confirmed to be single-phased, homogeneous, fine-grained (0.5–2 μm) and free of pores and microcracks. Previous wadsleyite and ringwoodite specimens hot-pressed by similar techniques (Gwanmesia et al. 1990) were shown to be elastically isotropic and exhibited no preferred orientation of the crystallites.

The bulk densities of the specimens were measured by the Archimedean technique involving immersion in distilled water (Gwanmesia et al. 2006). The densities (Table 1) are both within 0.2% of the X-ray density. We ground and polished the ends of each specimen to

Table 1 Length and aggregate elastic properties of pyrope specimens (#3741, #3813) measured before (bold) and after (italics) the high temperature measurements

Sample	Length (mm)	Density (g/cc)	V_p (km/s)	V_s (km/s)	G (GPa)	K (GPa)
3741	2.643	3.557	**9.09**	**5.12**	**93.2**	**169.6**
			8.97	*5.01*	*89.3*	*167.2*
3813	2.029	3.554	**9.04**	**5.07**	**91.4**	**168.6**
			9.06	*5.08*	*91.7*	*169.5*
Single crystal[a]			*9.10*	*5.13*	*94.0*	*169.4*

The X-ray density = 3.565 g/cc (Armbruster et al. 1992)

[a] Brillouin scattering data of Sinogeikin and Bass (2002)

be flat and parallel using 9, 6, 3 and 1 μm diamond paste in succession. The phase comparison method of ultrasonic interferometry (Jackson et al. 1981; Niesler and Jackson 1989) was used to measure the P wave and S wave travel times for the samples at room pressure and temperature, both before and after the high temperature experiments described below. P and S wave velocities (Table 1) are quite consistent for the two specimens (#3741, #3813). Moreover, with the exception of the S wave data after the high temperature run for #3741, all acoustic velocities from the two specimens were within 1% of the corresponding averages calculated from single crystal moduli measured by Brillouin spectroscopy (Sinogeikin and Bass 2002). This is good indication of the high acoustic quality of the polycrystalline specimens. Furthermore, agreement between the ''bench-top'' acoustic velocities before and after the high temperature experiments suggests that the samples were unaltered by temperature cycling.

High temperature acoustic velocity measurements

The high temperature acoustic P and S wave velocity measurements were conducted in an internally heated argon gas-medium pressure apparatus capable of reaching 300 MPa confining pressure. Details of this method are given by Jackson et al. (2005).

A primary internal component of the set up is a compound buffer rod of mild-steel and alumina that allows acoustic signals to be transmitted to and from the sample located in the high-temperature zone. The acoustic transducer is bonded to the free end of the steel buffer rod ensuring that the transducer remains stress-free and at room temperature when the sample is heated to high temperatures. Sample temperature is measured by a type-R thermocouple located within a jacketed hollow alumina assembly inserted through one end of the cylindrical pressure vessel.

In this study, we utilized the tapered alumina buffer rod configuration in order to minimize return to the transducer of energy that was not reflected from the buffer rod-sample interface (refer to Jackson et al. 2005 for further details). Secondly, the pyrope polycrystalline specimen in the pressure chamber was surrounded by cold-pressed NaCl to render the stress state of the sample as nearly hydrostatic as possible during heating. Gold layers of 1 μm thickness were vacuum-deposited at the interface between the steel and alumina buffer rods and also between the sample and the alumina to provide optimal mechanical coupling at these interfaces, once the temperature is raised at 300 MPa confining pressure.

Measurement of travel times of acoustic waves was accomplished by the phase comparison method of ultrasonic interferometry (Jackson et al. 1981; Niesler and Jackson 1989; Rigden et al. 1992). In this study, both longitudinal and shear wave signals were generated simultaneously by a dual mode (10° rotated Y-cut) $LiNbO_3$ transducer (see Kung et al. 2002; Sinelnikov et al. 2004) and detected by the source transducer.

Figure 1 shows the conditions of pressure and temperature achieved in the gas-apparatus acoustic experiments in this study and in the previous work of Gwanmesia et al. (2006) in the solid-medium apparatus. The gas apparatus containing the acoustic components was first sealed and pressurized to 300 MPa. Temperature was then increased slowly to 993 K. A progressive improvement in signal quality during pressurization and heating was attributed to improved coupling across the gold foil between buffer rod and specimen. Travel times of the acoustic P and S waves were subsequently measured at 50° intervals during the cooling cycle.

Results

In Table 2, we summarize the data obtained for the two pyrope specimens investigated in this study. Small corrections (2–8 ns for P waves, 2–5 ns for S waves) were applied to account for the effect on the travel times of the 1 μm gold bond between the sample and the buffer rod (Jackson and Niesler 1989). Travel times of acoustic waves at high T were then averaged across ranges of relatively high carrier frequency (40–60 MHz for P-wave and 28–40 MHz for S-wave) where the travel times are most nearly frequency independent. For both P and S waves, the fractional error in the measured travel times, estimated as twice the standard error in the mean, was of the order of 10^{-4} to 10^{-5}. After making small corrections to the sample temperature to compensate for the temperature gradient

Table 2 High temperature compressional (P) and shear (S) wave data

T (K)	l (mm)	ρ (g/cm^3)	t_p (μs)	t_s (μs)	V_p (km/s)	V_s (km/s)	M (GPa)	G (GPa)	K (GPa)
Pyrope specimen #3741									
298	2.643	3.560	0.5869	1.0393	9.01	5.09	288.8	92.1	166.0
325	2.644	3.558	0.5889	1.0404	8.98	5.08	286.8	91.9	164.3
378	2.645	3.553	0.5904	1.0438	8.96	5.07	285.2	91.2	163.5
429	2.646	3.548	0.5910	1.0463	8.95	5.06	284.4	90.8	163.4
480	2.647	3.543	0.5924	1.0476	8.94	5.05	283.0	90.5	162.4
531	2.648	3.538	0.5953	1.0502	8.90	5.04	280.1	90.0	160.1
582	2.650	3.533	0.5965	1.0513	8.88	5.04	278.9	89.8	159.2
634	2.651	3.528	0.5975	1.0546	8.87	5.03	277.7	89.2	158.8
686	2.652	3.522	0.5993	1.0575	8.85	5.02	276.0	88.6	157.8
739	2.654	3.517	0.6002	1.0610	8.84	5.00	275.0	88.0	157.6
791	2.655	3.511	0.6026	1.0646	8.81	4.99	272.6	87.4	156.2
841	2.657	3.506	0.6046	1.0674	8.79	4.98	270.7	86.9	154.9
890	2.658	3.500	0.6056	1.0697	8.78	4.97	269.7	86.4	154.4
941	2.659	3.495	0.6074	1.0731	8.76	4.96	268.0	85.9	153.5
993	2.661	3.489	0.6088	1.0773	8.74	4.94	266.6	85.1	153.1
Pyrope specimen #3813									
311	2.029	3.549	0.4495	0.7971	9.03	5.09	289.3	92.0	166.6
352	2.030	3.545	0.4512	0.7991	9.00	5.08	287.0	91.5	165.0
403	2.031	3.540	0.4525	0.8011	8.98	5.07	285.2	91.0	163.9
455	2.032	3.536	0.4537	0.8020	8.96	5.07	283.6	90.8	162.6
506	2.033	3.531	0.4549	0.8035	8.94	5.06	282.0	90.4	161.5
557	2.034	3.525	0.4560	0.8071	8.92	5.04	280.5	89.5	161.1
608	2.035	3.520	0.4574	0.8089	8.90	5.03	278.6	89.1	159.8
660	2.036	3.515	0.4586	0.8111	8.88	5.02	277.0	88.6	159.0
712	2.037	3.510	0.4599	0.8130	8.86	5.01	275.3	88.1	157.9
765	2.038	3.504	0.4612	0.8161	8.84	4.99	273.6	87.4	157.1
816	2.039	3.499	0.4623	0.8181	8.82	4.98	272.2	86.9	156.3
866	2.040	3.493	0.4638	0.8207	8.80	4.97	270.3	86.3	155.2
915	2.041	3.488	0.4652	0.8219	8.77	4.97	268.5	86.0	153.8
967	2.042	3.482	0.4667	0.8260	8.75	4.94	266.7	85.1	153.2
993	2.043	3.479	0.4672	0.8269	8.74	4.94	266.0	84.9	152.8

Also listed are temperature-corrected lengths and densities

between the sample and the thermocouple, high temperature sample densities and lengths were calculated using the independently measured thermal expansion data for pyrope via $l/l_0 = [1+\alpha\ (T-T_0)]^{1/3}$, ($\alpha = 2.3 \times 10^{-5} + 9.4 \times 10^{-9}\ T$, Wang et al. 1998). The effect of pressure is smaller by an order of magnitude and accordingly was neglected. Lengths, densities and average round trip travel times of the acoustic waves through the sample were subsequently used to calculate the velocities and elastic moduli at each temperature condition shown in Table 2.

In Fig. 2, we have plotted the P wave (2a) and S wave (2b) velocities as functions of temperature, for pyrope specimens #3741, and #3813. Given the uncertainties (10^{-4} to 10^{-5}) in travel times, the precision in these velocities is about twice that in the travel times and thus smaller than the symbol size in Fig. 2a and b. The small uncertainty in the specimen length ($<10^{-3}$) at ambient conditions has the capacity to produce a minor offset in the velocity–temperature trajectory but has no impact upon the temperature derivative. The decrease in velocities with temperature is reproducible and systematic for both specimens. The reproducibility of the velocity data between the two-polycrystalline specimens is also corroborated by the room P and T data displayed in Table 1. Specimen #3813 displayed interference patterns of higher quality than for #3741 and thus yielded more accurate determinations of acoustic wave travel times. Consequently, the bulk (K) and shear (G) modulus data for this specimen were fit linearly as a function of temperature (Fig. 3), yielding well-constrained temperature dependence of the bulk modulus $[(\partial Ks/\partial T)_P = -19.3(4)]$ and of the shear modulus $[(\partial G/\partial T)_P = -10.4(2)]$, with rms misfits of only 0.2%.

In Table 3, we compare the elastic moduli and their temperature dependence from this study with data from previous investigators. Our $(\partial Ks/\partial T)_P$ and $(\partial G/\partial T)_P$ values are in strong agreement with the acoustic data of Gwanmesia et al. (2006) as measured in a

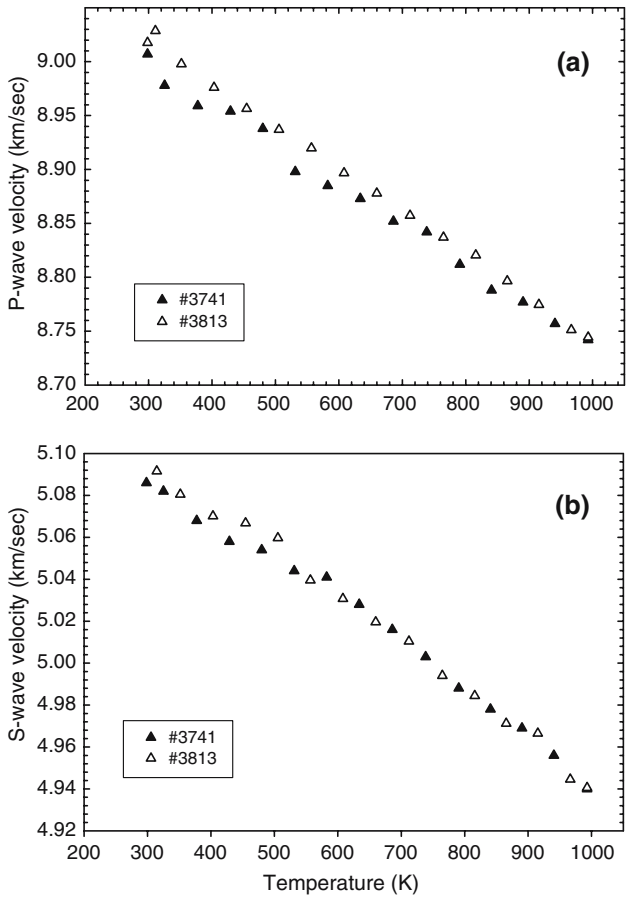

Fig. 2 Comparison of the variation of P wave (**a**) and S wave (**b**) velocities with temperature for polycrystalline pyrope specimens #3741 and #3813

DIA-type cubic anvil apparatus (SAM-85), in conjunction with synchrotron X-radiation, and also with the acoustic data of Suzuki and Anderson (1983) as measured by RPR on natural single crystal pyrope.

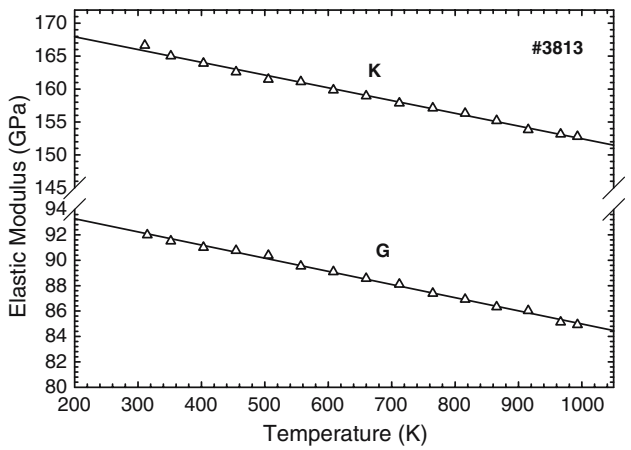

Fig. 3 Linear fit to bulk (K) and shear (G) modulus as a function of temperature at 300 MPa for sample #3813

Allowing for mutual measurement error, our determination of $(\partial G/\partial T)_P$ is consistent with that from the Brillouin scattering data of Sinogeikin and Bass (2002) on a natural pyrope single crystal, whereas our value for $(\partial K_S/\partial T)_P$ is not. Derivation of $(\partial K_T/\partial T)_P$ from measured $(\partial K_S/\partial T)_P$ data (or vice versa) requires differentiation with respect to temperature of the relationship $K_S = K_T(1 + \alpha\gamma T)$ requiring, in principle, a complete P–V–T equation-of-state (e. g., Jackson and Rigden 1996, Eq. B5). For the purpose of the comparisons in Table 3, however, an approximation based on pyrope data tabulated by Anderson and Isaak (1995) is employed. The $(\partial K_T/\partial T)_P$ values that we have calculated from our $(\partial Ks/\partial T)_P$ values are significantly larger in magnitude than those from the static compression studies of Wang et al. (1998) and Gwanmesia et al. (2006).

Discussion

The consistency between the ultrasonic data from this study and those of Gwanmesia et al. (2006) provides adequate justification for joint analysis of the two data sets in an effort to constrain the mixed derivatives ($\partial^2 K_s/\partial P\partial T$; $\partial^2 G/\partial P\partial T$). Although the gas- and solid-medium datasets display substantially different levels of scatter (~0.2 and ~1%, respectively: see Fig. 4), we have chosen to weight all data uniformly in the analysis of the combined dataset. Least-squares fitting of the combined dataset (Table 3, note 'f') yields $\mathrm{d}M/\mathrm{d}T$ values comparable with those for the separate fits of the gas- and solid-medium data, but with relatively low K_0 and high $\mathrm{d}K/\mathrm{d}P$, influenced by the gas- and solid-medium data, respectively. Slightly different values of K_0 and G_0 for the different specimens measured in the solid- and gas-medium apparatus may reflect minor differences in porosity, ultrasonic techniques and specimen size. Accordingly, for fits 'g' in Table 3, we chose to fix K_0 and G_0 for each data set at the value determined from the prior independent linear fit, and sought the optimal values of the first pressure and temperature derivatives for the combined data set (Table 3), initially with $\mathrm{d}^2M/\partial P\partial T$ set equal to zero. This strategy significantly reduced the rms misfit from 1.18 to 0.78% for K, but resulted in only a marginal improvement for G (0.81–0.78%). We plot (Fig. 4) the resulting modeled shear and bulk moduli versus the corresponding measured values, using data from the two different P and T regimes shown in Fig. 1. This analysis shows a very close correlation between measured and modeled moduli amongst the gas-medium data but greater scatter in the acoustic data from the

Table 3 300 K elastic moduli of pyrope and their temperature derivatives

K_S (GPa)	K_T (GPa)	G (GPa)	$(\partial K_S/\partial T)_P$ (MPa/K)	$(\partial K_T/\partial T)_P$ (MPa/K)	$(\partial G/\partial T)_P$ (MPa/K)	$(\partial K_S/\partial P)_T$ or $(K_T/\mathrm{d}P)_T$	$(\partial G/\partial P)_T$	$\partial^2 K_S/\partial P\partial T$ (10^{-3} K^{-1})	$\partial^2 G/\partial P\partial T$ (10^{-3} K^{-1})	Reference	Technique
171(2)	169.4(20)	94(2)	–14.0(20)	–19.4(30)	–9.2(10)	4.1(3)	1.3(2)			Sinogeikin and Bass (2000, 2002)	Brillouin (0–20 GPa; 300–1,100 K)
	170(2)			–21(2)						Wang et al. (1998)	PVT (0–11 GPa and 300–1,100 K)
171.2	169.4	92.6	–19.5[a]	–25.1[a]	–10.1[a]					Suzuki and Anderson (1983)	Acoustics (300–1,000 K)
171.2(11)	169.4	91.0(7)	–20.6(15)	–27[b]	–10.1(8)	4.55(20)	1.64(11)			Gwanmesia et al. (2006)	Acoustics (2–8 GPa and 300–1,100 K)
	167(4)			–22(2)[c]						Gwanmesia et al. (2006)	HTBM, P–V–T (2–8 GPa and 300–1100 K)
166.0(2)	164.3	92.2(1)	–19.3(4)	–26[b]	–10.4(2)					This study[e]	Acoustics (0.3 GPa and 300–1,000 K)
166.0(8)	164.3	91.6(3)	–20.7(15)	–27[b]	–10.2(5)	5.46(13)	1.54(5)			This study[f]	As above; joint acoustic analysis
(166.0) (171.2)		(92.2) (91.0)	–21.5(7)	–28[b]	–10.8(4)	4.61(8)	1.68(4)			This study[g]	Joint acoustic analysis
(166.0) (171.2)		(92.2) (91.0)	–21.9(8)	–28[b]	–11.2(5)	4.55(11)	1.63(6)	0.22(26)	0.20(14)	This study[h]	Joint acoustic analysis
(166.0) (171.2)		(92.2) (91.0)	[–19.3]	–26[b]	[–10.4]	4.53(12)	1.62(6)	–0.20(24)	0.07(12)	This study[i]	Joint acoustic analysis

[a] Average values of $(\partial K_T/\partial T)_P$ for the temperature interval 300–1,000 K calculated from the corresponding listed $(\partial K_S/\partial T)_P$ values using an approximation to $\{\partial[K_S/(1+\alpha\gamma T)]/\partial T\}_P$ and selected thermoelastic data from Anderson and Isaak (1995)

[b] Obtained from fit to data tabulated by Anderson and Isaak (1995)

[c] Obtained from fitting entire (excluding cold compression data) *P–V–T* data set simultaneously to high temperature Birch-Murnaghan (HTBM) equation of state, fixing K′ at 3.9

[d] Fitting each isothermal *P–V–T* data set separately

[e] Linear $M(T)$ fit data obtained in gas-medium high-pressure apparatus

[f] Joint analysis accomplished by simultaneous linear $M(P, T)$ fit to both gas- and solid-medium (Gwanmesia et al. 2006) $M(T)$ data sets without a priori constraint

[g] As for note[f]but with individual a priori constraints on M_0 from separate fits to gas- and solid-medium data

[h] As for note[g] with inclusion of additional term $(\mathrm{d}^2M/\mathrm{d}P\mathrm{d}T)P(T–300)$

[i] As for note [h] with additional a piori constraints on $\mathrm{d}M/\mathrm{d}T$ from the gas-medium fits (note e)

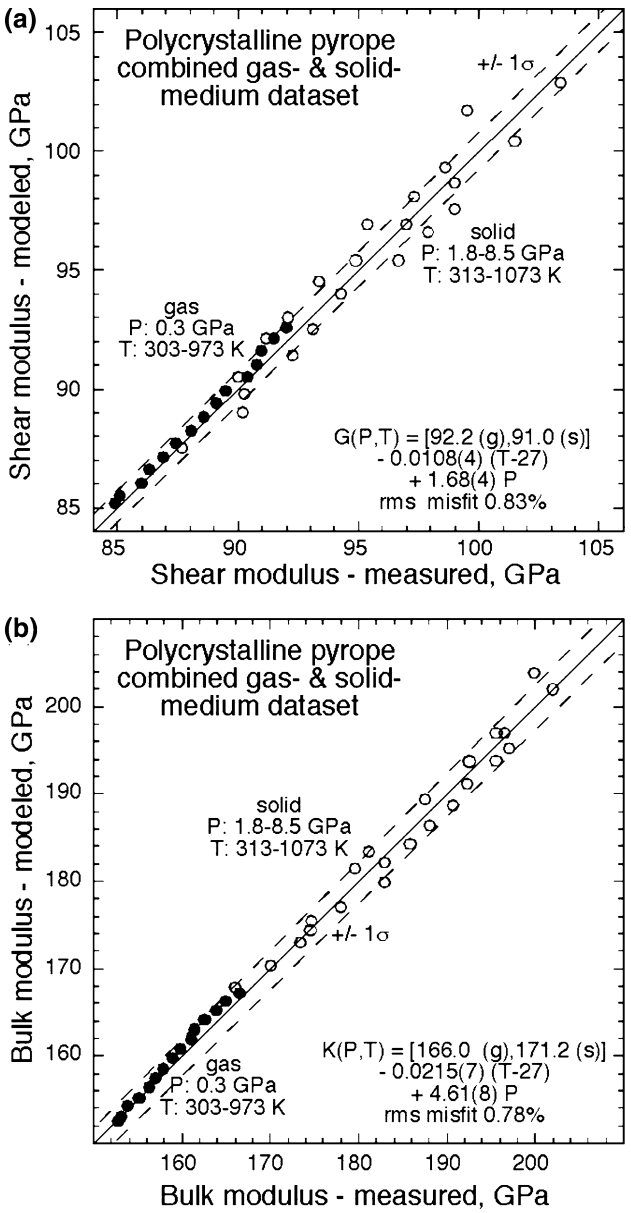

Fig. 4 Modeled shear (**a**) and bulk (**b**) moduli versus the corresponding measured values for data from gas-medium apparatus from this study and the cubic anvil multi-anvil high pressure apparatus (Gwanmesia et al. 2006)

solid-medium experiments. Finally, we sought to resolve the cross-derivatives of the elastic moduli from the joint analyses—with and without the prior constraints on dM/dT (fits 'i' and 'h', Table 3). Allowing non-zero values of $d^2M/\partial P\partial T$ produced no significant reduction of misfit. Inferred values of $\partial^2 G/\partial P\partial T$ [0.07(12), 0.20(14)] $\times 10^{-3}$ K^{-1} and $\partial^2 K_S/\partial P\partial T$ [–0.20(24), 0.22(26)] $\times 10^{-3}$ K^{-1}, though clearly of order 10^{-4} K^{-1}, are not significantly different from zero.

The greater precision of the moduli measured in the gas apparatus is attributable mainly to the larger sample volume, possibly augmented by more favorable signal/noise conditions associated with the narrow-band superheterodyne detection employed in the swept monochromatic phase comparison method of ultrasonic interferometry (Niesler and Jackson 1989). From the results of the joint analysis (Fig. 4), elastic moduli need to be measured in the cubic anvil apparatus with precision significantly better than 1% if the mixed derivatives of the elastic moduli are to be robustly extracted from such analyses of combined gas- and solid-medium data. The most recent data from the Stony Brook laboratory indicate that such precision is attainable (e. g., Liu et al. 2005; Li and Zhang 2005) with the transfer-function method on polycrystalline specimens of no more than 2 mm in diameter and 1 mm in length.

The conclusion from this analysis that the mixed derivatives are of order 10^{-4} K^{-1}, though not yet resolved with uncertainties less than 100%, can be evaluated by reference to the simplest models based on thermodynamic and lattice-dynamic considerations. A third-order Eulerian principal isotherm (300 K) with thermal pressure given by the Mie-Grüneisen-Debye formalism provides an adequate framework for the assimilation and assessment of data from both P–V–T and acoustic experiments (Jackson and Rigden 1996). Such a model, constructed for pyrope with the values of V_0, K_0, K'_0, Θ_0, γ_0, and q favored by Stixrude and Lithgow-Bertelloni (2005), provides predictions of the behavior of higher-order thermoelastic parameters. Evaluation of this model for the temperature interval 300–1,000 K at $P = 0$ yields temperature-averaged values of $(\partial K_S/\partial T)_P$ = –0.14(2) MPa K^{-1} and $(\partial K_T/\partial T)_P$ = –0.019 MPa K^{-1} reproduces the derivatives obtained from the data of Sinogeikin and Bass (2002; Table 3), on which it is based. For the temperature–pressure range of this study, an average value of $\partial^2 K_S/\partial T\partial P$ of 1.0×10^{-4} K^{-1} is inferred from the model, in general agreement with our experimental constraints.

It should be noted however, that optimal choice of parameters for the modeling of thermoelastic behavior is problematic. Stixrude and Lithgow-Bertelloni (2005) have reasonably accorded greatest weight to the latest elasticity data that pertains to the widest ranges of pressure and temperature. For pyrope, these were the single-crystal Brillouin spectroscopic studies of Sinogeikin and Bass (2000, 2002) to conditions of 20 GPa at room temperature and 1,100 K at ambient pressure, respectively. However, the Brillouin technique is typically less precise than ultrasonic interferometry by an order-of-magnitude. Moreover, there tends to be negative correlation between the width of the pressure range employed in elasticity studies and the inferred values of the pressure derivatives dM/dP. The values

reported by Sinogeikin and Bass for both $(\partial K_S/\partial P)_T$ and $(\partial G/\partial P)_T$ are substantially lower than the consensus values from acoustic studies of comparatively higher precision but with more limited pressure ranges. Adjustment of the Stixrude and Lithgow-Bertelloni (2005) model to match these latter observations, including those of the present study, would require substantially higher values of K' and q.

Conclusions

Two synthetic pyrope ($Mg_3Al_2SiO_4$) polycrystalline specimens of excellent acoustic quality have been hot-pressed in a 2,000 ton uniaxial split sphere apparatus at 9 GPa and 1,273 K, and their elastic wave velocities measured to ~1,000 K at 300 MPa, in an internally heated gas-medium high pressure apparatus, using the phase comparison method of ultrasonic interferometry. Temperature dependence of the elastic bulk modulus $[(\partial Ks/\partial T)_P = -19.3(4)$ MPa $K^{-1}]$ and of the shear modulus $[(\partial G/\partial T)_P = -10.4(2)$ MPa $K^{-1}]$ obtained from this study show remarkable agreement with previous acoustic measurements on synthetic polycrystalline pyrope in a solid-medium cubic anvil apparatus (Gwanmesia et al. 2006) and on a natural single crystal tested at ambient pressure by the RPR (Suzuki and Anderson 1983). However, a significantly lower value of $|(\partial Ks/\partial T)_P| = 0.14(2)$ MPa K^{-1} has been reported from a Brillouin scattering study of single-crystal pyrope (Sinogeikin and Bass 2002). Joint analysis of data from this study and from Gwanmesia et al. (2006) yield $\partial^2 K_s/\partial P\partial T$ and $\partial^2 G/\partial P\partial T$ of order 10^{-4} K^{-1} with uncertainties of about 100%. Tighter constraints on the cross derivatives of elastic moduli will require improved precision of ultrasonic measurements at simultaneously high temperature and pressure within diamond-anvil or multi-anvil apparatus.

Acknowledgments We thank Craig Saint for assistance with laboratory work. This research was supported by funding from the Australian Research Council (LX0348106) and partially by a NSF grant (INT 02-33849) to R. C. Liebermann for a collaborative research program with the Australian National University. We thank S. Jacobsen for a thorough and constructive review of the original version of this paper. This is Mineral Physics Institute Publication No. 368.

References

Anderson OL, Isaak DG (1995) Elastic constants of mantle minerals at high temperatures In: Ahrens TJ (ed) Mineral physics and crystallography: a handbook of physical constants. AGU, Washington, pp 64–97

Armbruster TC, Geiger A, Lager GA (1992) Single-crystal X-ray structure and study of synthetic pyrope almandine garnets at 100 and 293 K. Am Min 77:512–521

Chen G, Liebermann RC, Weidner DJ (1998) Elasticity of single crystal MgO to 8 Gigapascals and 1,600 Kelvin. Science 280:1913–1916

Chen G, Cooke JA Jr, Gwanmesia GD, Liebermann RC (1999) Elastic wave velocities of $Mg_3Al_2Si_3O_{12}$-pyrope garnet to 10 GPa. Am Min 84:384–388

Gasparik T (1990) Phase relations in the transition zone. J Geophys Res 95:15751–15769

Gasparik T (1992) Melting experiments on the enstatite–pyrope join at 80–152 kbar. J Geophys Res 97:15181–15188

Gwanmesia GD, Liebermann RC (1992) Polycrystals of high pressure phases of mantle minerals: hot-pressing and characterization of physical properties. In: Syono Y, Manghnani MH (eds) High-pressure research: application to the earth and planetary sciences. TERRAPUB, Tokyo/American Geophysical Union, Washington, DC, 117–135

Gwanmesia GD, Liebermann RC, Guyot F (1990) Hot-pressing and characterization of polycrystals of β-Mg_2SiO_4 for acoustic velocity measurements. Geophys Res Lett 17:1331–1334

Gwanmesia GD, Li B, Liebermann RC (1993) Hot pressing of high pressure phases of mineral phases of mantle minerals in multi anvil apparatus. PAGEOPH 141:467–484

Gwanmesia GD, Zhang J, Darling K, Kung J, Li B, Wang L, Neuville D, Liebermann RC (2006) Elasticity of polycrystalline pyrope ($Mg_3Al_2Si_3O_{12}$) to 9 GPa and 1,000°C. Phys Earth Planet Inter 155:179–190

Isaak DG (1993) The mixed P–T derivatives of elastic moduli and implications on extrapolating throughout Earth's mantle. Phys Earth Planet Inter 80:347–348

Jackson I, Rigden SM (1996) Analysis of P–V–T data: constraints on the thermoelastic properties of high-pressure minerals. Phys Earth Planet Inter 96:85–112

Jackson I, Niesler H, Weidner DJ (1981) Explicit correction of ultrasonically determined elastic wave velocities for transducer-bond phase shift. J Geophys Res 86:3736–3748

Jackson I, Webb S, Weston L, Boness D (2005) Frequency dependence of the elastic wave speeds at high temperature: a direct experimental demonstration. Phys Earth Planet Inter 148:85–96

Kawai N, Endo S (1970) The generation of ultrahigh hydrostatic pressures by a split-sphere apparatus. Rev Sci Instrum 41:1178–1181

Kawai N, Togaya M, Onodera A (1973) A new device for pressure vessels. Proc Jpn Acad 49:623–626

Kung J, Li B, Weidner DJ, Zhang J, Liebermann RC (2002) Elasticity of $(Mg_{0.83}, Fe_{0.17})O$ ferropericlase at high pressure: ultrasonic measurements in conjunction with X-radiation techniques. Earth Planet Sci Lett 203:227–566

Leitner BJ, Weidner DJ, Liebermann RC (1980) Elasticity of single crystal pyrope and implications for garnet solid solution series. Phys Earth Planet Inter 22:111–121

Li B, Zhang J (2005) Pressure and temperature dependence of elastic wave velocity of $MgSiO_3$ perovskite and the composition of the lower mantle. Phys Earth Planet Inter 151:143–154

Liu W, Kung J, B Li (2005) Elasticity of San Carlos olivine to 8 GPa and 1,073 K. Geophys Res Lett 32:L16301

Niesler H, Jackson I (1989) Pressure derivatives of elastic wave velocities from ultrasonic interferometric measurements on jacketed polycrystals. J Acoust Soc Am 86:1573–1585

Rigden SM, Gwanmesia GD, Jackson I, Liebermann RC (1992) Progress in high pressure ultrasonic interferometry: the pressure dependence of elasticity of Mg_2SiO_4 polymorphs and constraints on the composition of the transition zone

of the Earth's mantle. In: Syono Y, Manghnani MH (eds) High-pressure research: application to the earth and planetary sciences. TERRAPUB, Tokyo/American Geophysical Union, Washington, DC 167–182

Rigden SM, Gwanmesia GD, Liebermann RC (1994) Elastic wave velocities of a pyrope–majorite garnet to 3 Gpa. Phys Earth Planet Inter 86:35–44

Sinelnikov YD, Chen G, Liebermann RC (2004) Dual mode ultrasonic interferometry in multi-anvil, high-pressure apparatus using single-crystal olivine as the pressure standard. Int J High Press Res 24:183–191

Sinogeikin SV, Bass JD (2000) Single-crystal elasticity of pyrope and MgO to 20 GPa by Brillouin scattering in the diamond cell. Phys Earth Planet Inter 120:43–62

Sinogeikin SV, Bass JD (2002) Elasticity of pyrope and majorite–pyrope solid solutions to high temperatures. Phys Earth Planet Inter 203:549–555

Spetzler HA (1970) Equation of state of polycrystalline and single crystal MgO to 8 kilobars and 800 K. Geophys Res 75:2073–2087

Stixrude L, Lithgow-Bertelloni C (2005) Thermodynamics of mantle minerals: 1. Physical properties. Geophys J Int 162:610–632

Suzuki I, Anderson OL (1983) Elasticity and thermal expansion of a natural garnet up to 1,000 K. J Phys Earth 31:125–138

Wang Y, Weidner DJ, Zhang J, Gwanmesia GD, Liebermann RC (1998) Thermal equation of state of garnets along the pyrope–majorite join. Phys Earth Planet Inter 105:59–71

Yagi T (2001) KAWAI-type apparatus. Rev High Press Sci Technol 11:171